

Refine and Purify: Orthogonal Basis Optimization with Null-Space Denoising for Conditional Representation Learning

Jiaquan Wang¹ Yan Lyu¹ Chen Li² Yuheng Jia¹

Abstract

Conditional representation learning aims to extract criterion-specific features for customized tasks. Recent studies project universal features onto the conditional feature subspace spanned by an LLM-generated text basis to obtain conditional representations. However, such methods face two key limitations: sensitivity to subspace basis and vulnerability to inter-subspace interference. To address these challenges, we propose OD-CRL, a novel framework integrating Adaptive Orthogonal Basis Optimization (AOBO) and Null-Space Denoising Projection (NSDP). Specifically, AOBO constructs orthogonal semantic bases via singular value decomposition with a curvature-based truncation. NSDP suppresses non-target semantic interference by projecting embeddings onto the null space of irrelevant subspaces. Extensive experiments conducted across customized clustering, customized classification, and customized retrieval tasks demonstrate that OD-CRL achieves a new state-of-the-art performance with superior generalization.

1. Introduction

Representation learning is a fundamental paradigm in machine learning that extracts meaningful abstractions from raw data. Enabled by self-supervised techniques such as contrastive learning (Chen et al., 2020; He et al., 2020; Caron et al., 2020) and masked prediction (Devlin et al., 2019; He et al., 2022; Wei et al., 2022), representation learning has been successfully applied to multiple downstream tasks (Mo et al., 2022; Gordo et al., 2016; Sarafianos et al., 2019; Yan et al., 2023). However, a critical challenge persists: existing feature learning methods predominantly capture dominant features (e.g., shape and category) while overlooking other

¹School of Computer Science and Engineering, Southeast University, China ²Biomedicine Discovery Institute, Department of Biochemistry and Molecular Biology, Monash University, Australia. Correspondence to: Yuheng Jia <yhjia@seu.edu.cn>.

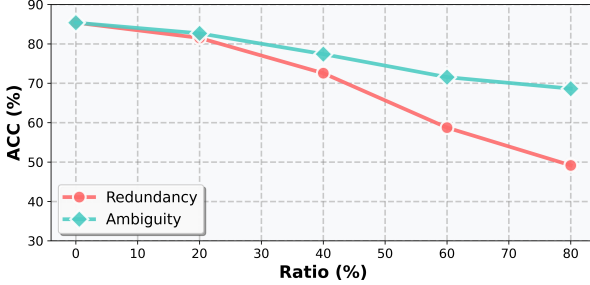
Preprint. February 6, 2026.

secondary features (e.g., color and quantity). This limitation constrains the applicability of representation learning to customized tasks with specific criteria. For instance, when clustering images by color similarity, conventional methods may inadvertently group objects based on their shapes, failing to meet the user-specified criterion.

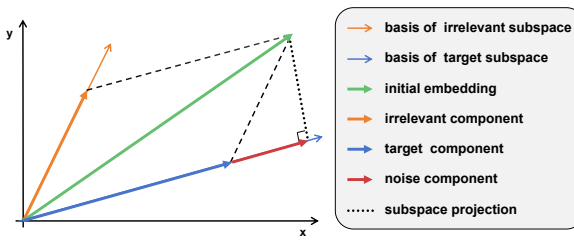
Consequently, conditional representation learning has emerged as a promising paradigm that extracts criterion-specific representations tailored to particular requirements. Supervised fine-tuning methods (Geng et al., 2025; Liu et al., 2024) obtain conditional representations by retraining models on criterion-aligned labeled data. Prompt-driven methods (Kwon et al., 2023; Wang et al., 2025) typically rely on meticulously crafted prompts to elicit conditional representations from LLMs. However, supervised methods require expensive data annotation, while prompt-driven approaches incur heavy inference burdens from LLMs.

Recently, subspace projection-based methods (Yao et al., 2024b;a; Liu et al., 2025) have been employed to achieve efficient conditional representation learning. Specifically, criterion-specific text bases are firstly constructed by encoding LLM-generated descriptions through a VLM’s text encoder, while images are simultaneously transformed into general representations via the image encoder. The resulting image embeddings are then projected onto the subspaces spanned by criterion-specific text bases to obtain conditional representations.

However, such methods face two critical limitations that hinder their effectiveness. First, they are highly sensitive to the quality of LLM-generated text bases. Specifically, the presence of highly correlated synonyms (e.g., “red”, “crimson”) and polysemous words (e.g., “orange”, “rose”) in LLM-generated texts introduces semantic redundancy and ambiguity into the resulting bases for projection. As shown in Figure 1(a), such semantic redundancy and ambiguity in bases substantially degrade the discriminability of learned conditional representations. Therefore, a general optimization strategy for text bases is essential to enhance projection performance. Second, existing methods assume mutual orthogonality between criterion-specific subspaces during projection, neglecting the inter-subspace interference. However, this assumption is frequently invalidated in practice,



(a) Clustering performance with different ratios of low-quality basis



(b) Interference between non-orthogonal subspaces

Figure 1. Sensitivity to subspace basis and vulnerability to inter-subspace interference constitute critical limitations in current subspace projection-based methods. (a) As the ratio of low-quality bases containing redundancy or ambiguity increases, clustering performance declines. (b) Noise components induced by subspace non-orthogonality lead to projection deviation.

as subspaces corresponding to different criteria inevitably exhibit overlap in feature space. Figure 1(b) illustrates the projection deviation induced by this non-orthogonality of subspaces, showing the necessity of eliminating interference from non-target semantic components.

In this paper, we propose a novel method called OD-CRL, which comprises two key components: Adaptive Orthogonal Basis Optimization (AOBO) and Null-Space Denoising Projection (NSDP). Specifically, AOBO automatically constructs an orthogonal semantic basis from LLM-generated text via singular value decomposition (SVD). To balance information preservation and noise suppression, AOBO adopts a curvature-based truncation to determine the optimal number of basis vectors. NSDP is designed to explicitly suppress interference from non-target semantic components. By projecting image embeddings onto the null space of non-target subspaces prior to conditional representation extraction, NSDP ensures that the learned representations remain pure and criterion-specific. Extensive experiments across diverse tasks, including customized clustering, customized classification, and customized retrieval, demonstrate that OD-CRL achieves superior performance with strong generalization.

In summary, our contributions are as follows:

- We propose Adaptive Orthogonal Basis Optimization, which constructs orthogonal semantic bases from LLM-generated text through SVD with a curvature-based adaptive truncation, effectively enhancing the discriminability of conditional representations.
- We introduce Null-Space Denoising Projection to suppress non-target semantic interference. By projecting embeddings onto the null space of irrelevant subspaces, NSDP ensures the purity and specificity of the learned conditional representations.
- Extensive experiments show that OD-CRL achieves state-of-the-art performance on diverse downstream tasks, including customized clustering, customized classification, and customized retrieval, advancing efficient conditional representation learning.

2. Related Work

2.1. General Representation Learning

General representation learning aims to extract universal features from raw data. As a classical unsupervised learning method, autoencoders (Hinton & Salakhutdinov, 2006) obtain compact representations by minimizing reconstruction error. Denoising autoencoders (Vincent et al., 2008) and variational autoencoders (Kingma & Welling, 2013) introduce corruption robustness and probabilistic modeling respectively, improving latent space stability and structure. In recent years, the self-supervised learning paradigm has significantly expanded the boundaries of representation learning. Pretext tasks such as patch and rotation prediction (Doersch et al., 2015; Gidaris et al., 2018), solving jigsaw puzzles (Noroozi & Favaro, 2016), and colorization (Zhang et al., 2016) enable models to capture global-local consistency. Contrastive learning frameworks such as SimCLR (Chen et al., 2020), MoCo (He et al., 2020), and SwAV (Caron et al., 2020) employ instance discrimination to learn highly discriminative features without manual annotation. CLIP (Radford et al., 2021) aligns visual and language spaces through cross-modal contrastive learning, while BLIP-2 (Li et al., 2023) bridges frozen unimodal models via contrastive learning with a lightweight Querying Transformer. Both have become mainstream feature extractors for downstream tasks. Despite significant advances, most existing representation learning methods focus solely on dominant features. The neglect of diverse conditional features limits their applicability to customized tasks.

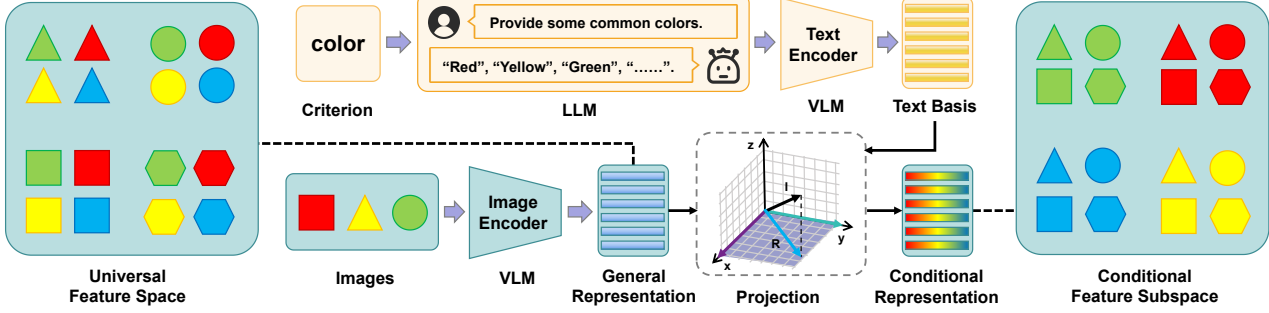


Figure 2. The basic pipeline of subspace projection-based conditional representation learning.

2.2. Conditional Representation Learning

Conditional representation learning aims to extract criterion-specific features from raw data. Supervised fine-tuning (Geng et al., 2025; Liu et al., 2024) provides a straightforward solution by retraining pre-trained models on criterion-specific labeled datasets. However, this approach is fundamentally constrained by data scarcity and prohibitive labeling costs. To mitigate reliance on labeled data, recent methods leverage expert models to elicit conditional representations through carefully designed prompts. IC|TC (Kwon et al., 2023) obtains conditional labels for images via direct dialogue with VLMs, while ESMC (Wang et al., 2025) captures intermediate hidden states from VLMs that exhibit the strongest response to target criteria as conditional representations. Nevertheless, the substantial computational overhead and sensitivity to prompt design remain significant bottlenecks. Subspace projection-based methods construct conditional representations by projecting image embeddings onto subspaces spanned by criterion-specific text bases. Multi-Map (Yao et al., 2024b) and Multi-Sub (Yao et al., 2024a) learn a set of trainable text basis weights for each image, which are optimized jointly through cross-modal alignment objectives. Upon convergence, these learned weights encode the image information within the specified semantic subspace. CRL (Liu et al., 2025) directly employs cosine similarity between image features and text basis vectors as conditional representations. However, the performance of projection is severely limited by the quality of LLM-generated text bases and interference from irrelevant semantic components.

3. Method

3.1. Formulation and Framework

Given a set of images $\mathbf{X} = \{x_1, x_2, \dots, x_m\}$ and a user-specified criterion C (e.g., ‘‘color’’ or ‘‘texture’’), conditional representation learning aims to extract image representations that are aligned with C .

As shown in Figure 2, conditional representation learning is formulated as a subspace projection process on feature representations. The key insight is to construct a target feature subspace corresponding to C and project the image features onto this subspace to obtain criterion-specific representations.

To construct the basis under the specific criterion C , we query an LLM to generate the related descriptive text W :

$$W = \text{LLM}(P_1, C) \quad (1)$$

where P_1 denotes the LLM prompt template.

The generated text W is then encoded by a Vision-Language Model (VLM) to obtain a set of linearly independent basis vectors \mathbf{T} that span the feature subspace corresponding to criterion C :

$$\mathbf{T} = \text{VLM}_{\text{text}}(P_2, W) \quad (2)$$

where P_2 denotes the VLM prompt that is concatenated with W to construct a complete sentence. More details about the text basis generation can be found in Appendix A.

In parallel, images \mathbf{X} are encoded through the same VLM to extract their universal features \mathbf{I} :

$$\mathbf{I} = \text{VLM}_{\text{image}}(\mathbf{X}) \quad (3)$$

Finally, the conditional representations \mathbf{R} are obtained by projecting the universal features \mathbf{I} onto the conditional feature subspace spanned by \mathbf{T} :

$$\mathbf{R} = \text{proj}(\mathbf{I}, \mathbf{T}) \quad (4)$$

Through this projection, \mathbf{R} capture only the information relevant to the specified criterion C , enabling criterion-specific image analysis.

3.2. Adaptive Orthogonal Basis Optimization

While current methods directly utilize LLM-generated text to construct the projection basis for conditional representation learning, such descriptive texts often exhibit semantic

redundancy and ambiguity. Specifically, when an LLM is queried about color-related expressions, the generated text may include highly correlated terms such as “red”, “crimson” and “scarlet”, which map to nearly identical semantic directions in the VLM’s feature space. Moreover, polysemous words such as “orange” and “rose” may inadvertently introduce unintended semantic information beyond the target criterion. Such redundancy and ambiguity are encoded in the projection basis, which compromises the discriminability of the learned representations. To address this limitation, we propose Adaptive Orthogonal Basis Optimization, which automatically constructs an orthogonal basis from LLM-generated text.

SVD-based Basis Optimization. Given the original text basis $\mathbf{T} \in \mathbb{R}^{n \times d}$, where n denotes the number of descriptive texts and d represents the embedding dimension, we perform singular value decomposition:

$$\mathbf{T} = \mathbf{U} \boldsymbol{\Sigma} \mathbf{V}^\top \quad (5)$$

where $\mathbf{U} \in \mathbb{R}^{n \times n}$ and $\mathbf{V} \in \mathbb{R}^{d \times d}$ are orthogonal matrices, and $\boldsymbol{\Sigma} \in \mathbb{R}^{n \times d}$ is a diagonal matrix containing the singular values in descending order.

The column vectors of \mathbf{V} form an orthonormal basis that spans the criterion-specific feature subspace induced by the original text embeddings. The orthogonality ensures that each basis vector represents a decorrelated semantic component, thereby eliminating redundancy among the text embeddings.

Curvature-based Adaptive Truncation. However, not all basis vectors in \mathbf{V} encode meaningful semantics. Basis vectors corresponding to larger singular values capture discriminative information, whereas those with smaller singular values primarily represent noise introduced by redundancy and ambiguity. To balance semantic information preservation against noise removal, we adopt a curvature-based truncation to automatically determine the optimal number k^* of basis vectors to retain.

Specifically, we compute the cumulative energy ratio:

$$E(k) = \frac{\sum_{i=1}^k \sigma_i^2}{\sum_{i=1}^n \sigma_i^2} \quad (6)$$

where σ_i denotes the i -th singular value. The cumulative energy curve $E(k)$ typically exhibits an “elbow” shape: it rises steeply as principal components capture most variance, then flattens as subsequent components contribute diminishing information.

To quantify this “elbow” behavior, we construct a normalized discrete curve (x_i, y_i) for $i = 1, 2, \dots, n$, where $x_i = (i - 1)/(n - 1) \in [0, 1]$ represents the normalized proportion of retained basis vectors, and y_i is the min-max

normalized cumulative energy derived from $E(k)$:

$$y_i = \frac{E(i) - E(1)}{E(n) - E(1)} \in [0, 1] \quad (7)$$

The curvature at each point is then computed as:

$$\kappa(x_i) = \frac{|y''(x_i)|}{(1 + (y'(x_i))^2)^{3/2}} \quad (8)$$

where $y'(x_i)$ and $y''(x_i)$ are estimated via finite differences. The optimal k^* corresponds to the point of maximum curvature:

$$k^* = \arg \max_i \kappa(x_i) \quad (9)$$

The maximum curvature point identifies the location where the marginal energy gain per additional component decreases most rapidly, marking the transition from signal-dominated to noise-dominated directions. This adaptive truncation ensures retention of sufficient semantic information while effectively filtering out noise-contaminated dimensions.

Finally, we construct the optimized orthogonal basis $\mathbf{T}^* \in \mathbb{R}^{k^* \times d}$ by selecting the top k^* right singular vectors:

$$\mathbf{T}^* = \mathbf{V}_{:,1:k^*}^\top \quad (10)$$

which serves as the semantic basis for subsequent projection.

The optimized basis possesses several key advantages: (1)

Orthogonality: The basis vectors significantly eliminate redundancy ($\text{rank}(\mathbf{T}^*) \ll \text{rank}(\mathbf{T})$) while reducing projection to inner product computation; (2) **Optimality:** For any given k^* , the retained basis vectors explain the maximum possible variance in the target subspace, yielding highly discriminative projected representations; (3) **Robustness:** The basis vectors effectively separate signal from noise introduced by redundancy and ambiguity, filtering out contaminated dimensions while preserving discriminative components.

3.3. Null-Space Denoising Projection

In practice, feature subspaces corresponding to different criteria are not orthogonal. Consequently, criterion-specific projections remain susceptible to interference from irrelevant semantic components in other non-orthogonal subspaces. To further purify the conditional representations, we propose Null-space Denoising Projection that explicitly suppresses such interference.

Semantic Subspace Decomposition. We formally define two subspaces within the feature space. The target subspace, spanned by \mathbf{T}_t^* , captures features aligned with the user-specified criterion. The noise subspace encompasses all non-target semantic components, defined as the union of

subspaces corresponding to non-target criteria. Under this framework, the image embeddings can be decomposed as:

$$\mathbf{I} = \mathbf{R}_t \mathbf{T}_t^* + \mathbf{R}_n \mathbf{T}_n^* + \epsilon \quad (11)$$

where $\mathbf{I} \in \mathbb{R}^{m \times d}$ denotes the init image embeddings from the VLM, $\mathbf{T}_t^* \in \mathbb{R}^{k^* \times d}$ is the target subspace basis, $\mathbf{R}_t \in \mathbb{R}^{m \times k^*}$ denotes the target-aligned representations, $\mathbf{T}_n^* \in \mathbb{R}^{p \times d}$ is the noise subspace basis, $\mathbf{R}_n \in \mathbb{R}^{m \times p}$ denotes the non-target representations, and $\epsilon \in \mathbb{R}^{m \times d}$ captures the residual.

Null-Space Projection. To eliminate feature components aligned with non-target semantics, we project the image embeddings onto the null space (orthogonal complement) of the noise subspace. We firstly perform SVD to identify the null space of the noise subspace:

$$\mathbf{T}_n^* = \mathbf{U}_n \Sigma_n \mathbf{V}_n^\top \quad (12)$$

where $\mathbf{T}_n^* \in \mathbb{R}^{p \times d}$ represents the noise subspace basis, approximated by the optimized basis of the non-target dominant subspace (e.g., shape for color-based tasks). $\mathbf{V}_n \in \mathbb{R}^{d \times d}$ contains the right singular vectors, and $\Sigma_n \in \mathbb{R}^{p \times d}$ contains the singular values in descending order. Let $r = \text{rank}(\mathbf{T}_n^*)$ denote the numerical rank. The null space of \mathbf{T}_n^* is spanned by the trailing $(d - r)$ right singular vectors:

$$\mathbf{T}_{\text{null}} = \mathbf{V}_{:,r+1:d}^\top \in \mathbb{R}^{(d-r) \times d} \quad (13)$$

where \mathbf{T}_{null} consists of all vectors orthogonal to the noise subspace. Following the standard subspace projection formula, the denoised image representation is computed as:

$$\tilde{\mathbf{I}} = \mathbf{I} \mathbf{T}_{\text{null}}^\top (\mathbf{T}_{\text{null}} \mathbf{T}_{\text{null}}^\top)^{-1} \mathbf{T}_{\text{null}} = \mathbf{I} \mathbf{T}_{\text{null}}^\top \mathbf{T}_{\text{null}} \quad (14)$$

The null-space projection eliminates components of \mathbf{I} in the span of \mathbf{T}_n^* , ensuring that semantic components residing in the noise subspace do not contaminate the subsequent target subspace projection.

Conditional Representation Extraction. Finally, we extract the conditional representation by projecting the denoised image features $\tilde{\mathbf{I}}$ onto the target subspace spanned by \mathbf{T}_t^* :

$$\mathbf{R}_t = \tilde{\mathbf{I}} (\mathbf{T}_t^*)^\top \in \mathbb{R}^{m \times k^*} \quad (15)$$

The obtained \mathbf{R}_t are criterion-specific representations that encode target-relevant semantics while remaining free from interference by the noise subspace.

Notably, due to the non-orthogonality of subspaces, Null-Space Denoising Projection inevitably removes a portion of target semantic components that lie in the subspace overlapping regions when eliminating irrelevant ones. Nevertheless, we demonstrate in Appendix B that the gain from noise reduction substantially outweighs this loss.

4. Experiments

To evaluate the performance of the proposed OD-CRL, we apply the method to three downstream tasks including customized clustering, customized few-shot classification, and customized fashion retrieval. Given the focus on conditional representation learning, these tasks employ diverse evaluation criteria and feature-rich datasets to ensure comprehensive assessment. We further conduct ablation studies, visualizations, and analysis on text basis to demonstrate the effectiveness and robustness of the proposed method.

4.1. Customized Clustering

Dataset. For this task, we employ Clevr4-10k (Vaze et al., 2023) and Cards (Yao et al., 2023) as benchmark datasets. Clevr4-10k is a synthetic dataset containing 10,531 samples with 4 distinct partition criteria based on “shape”, “texture”, “color”, and “count”, respectively. Cards is a poker card dataset comprising 8,029 samples, organized according to 2 criteria, namely “number” and “suit”.

Setup. We utilize pre-trained CLIP to extract initial representations from text and images. Subsequently, we perform k-means clustering on the learned conditional representations, repeating the procedure 20 times with different random seeds, and report the average results. BLIP2-based experiments are also incorporated to demonstrate the generalizability of OD-CRL.

Metric. We employ three widely used clustering metrics for evaluation: Normalized Mutual Information (NMI), Accuracy (ACC), and Adjusted Rand Index (ARI).

Performance. As shown in Table 1, the conditional representations derived from OD-CRL exhibit remarkable clustering performance improvements over the general representations from original CLIP, especially for the color criterion, where the ACC is substantially boosted from 12.23% to 89.88%. OD-CRL significantly surpasses all other customized clustering methods across all criteria. When using CLIP as the backbone, OD-CRL achieves an average performance improvement of 26.08% over CRL across all evaluation metrics. Moreover, without complex clustering modules, it achieves near-optimal performance even for the shape criterion, where traditional clustering methods (Li et al., 2021; Van Gansbeke et al., 2020) typically perform best. Remarkably, OD-CRL accomplishes this without requiring any training, effectively balancing efficiency with superior performance.

4.2. Customized Few-shot Classification

Dataset. Similar to customized clustering, we continue to use the Clevr4-10k and Cards datasets to evaluate OD-CRL’s performance on customized few-shot classification.

Table 1. Performance on the task of customized clustering.

Method	Clevr4-10k										Mean	
	Texture			Shape			Color					
	NMI	ACC	ARI	NMI	ACC	ARI	NMI	ACC	ARI			
CC	0.16	11.34	0.00	94.66	96.89	93.90	16.54	11.42	0.07	36.11		
SCAN	0.41	11.97	0.86	90.99	89.10	84.03	0.20	11.51	0.01	32.12		
Multi-Map	3.77	17.25	1.81	67.48	66.01	57.40	56.83	56.46	45.73	41.42		
Multi-Sub	4.93	18.30	3.52	72.48	72.07	61.48	64.34	62.19	59.62	46.55		
CLIP	1.11	13.09	0.41	74.22	73.19	64.15	0.83	12.23	0.27	26.61		
CLIP+CRL	10.91	25.22	6.55	78.40	81.83	71.35	88.09	87.26	81.07	58.96		
CLIP+OD-CRL	14.11	28.42	8.81	86.67	90.69	84.11	89.99	89.88	85.09	64.19		
BLIP2	0.79	12.32	0.28	86.98	85.68	81.17	0.99	11.92	0.24	31.15		
BLIP2+CRL	6.29	18.85	3.76	90.01	87.97	83.35	83.44	81.78	74.37	58.87		
BLIP2+OD-CRL	7.98	20.80	5.02	93.20	93.01	90.26	88.86	90.39	83.68	63.69		

Method	Clevr4-10k										Mean	
	Count			Number			Suits					
	NMI	ACC	ARI	NMI	ACC	ARI	NMI	ACC	ARI			
CC	2.08	14.67	1.09	24.91	26.34	12.30	24.94	39.21	16.87	18.05		
SCAN	3.42	14.29	1.23	11.11	18.21	17.60	15.01	32.02	9.48	13.60		
Multi-Map	11.38	20.13	7.67	16.32	20.61	7.95	14.02	46.65	11.08	17.31		
Multi-Sub	13.77	21.64	9.28	19.58	23.27	10.28	18.76	49.09	15.24	20.10		
CLIP	9.50	19.02	5.70	16.84	18.91	8.44	16.52	43.74	12.93	16.84		
CLIP+CRL	25.51	26.29	12.52	24.68	28.59	12.27	37.70	62.08	34.36	29.33		
CLIP+OD-CRL	28.47	29.76	15.47	38.78	44.45	28.40	41.61	73.22	42.20	38.04		
BLIP2	6.11	16.36	3.13	24.34	25.25	13.08	31.26	47.04	22.25	20.98		
BLIP2+CRL	20.17	25.16	10.73	46.40	48.55	33.47	59.43	71.96	53.00	40.99		
BLIP2+OD-CRL	26.17	29.77	15.23	58.07	61.90	48.76	62.52	83.33	62.71	49.83		

Setup. Consistent with Section 4.1, CLIP is used to extract initial representations for OD-CRL. To ensure fair comparison, we employ the logistic regression function from the scikit-learn package for few-shot learning, with 1, 5, and 10 samples per class, respectively. To mitigate the impact of randomness, we perform 20 random selections of training data for each experimental setting and report the average results. BLIP2-based experiments are also incorporated to demonstrate the generalizability of OD-CRL

Metric. For the task of customized few-shot classification, we adopt accuracy as the evaluation metric.

Performance. Table 2 demonstrates the effectiveness of OD-CRL on customized few-shot classification. Compared to vanilla CLIP, OD-CRL achieves substantial improvements, with an average gain of 46.23% across all settings. Against the strong baseline CRL, OD-CRL consistently delivers superior performance, particularly when training examples are extremely limited. Notably, for color-based classification on Clevr4-10k, CLIP+OD-CRL achieves a 25.44% improvement over CLIP+CRL in the 1-shot setting. These consistent performance gains confirm OD-CRL’s ability to extract discriminative conditional representations that effectively align with specific criteria.

4.3. Customized Fashion Retrieval

Dataset. Following prior work (Ma et al., 2020), we adopt the category and attribute prediction benchmark from Deep-Fashion (Liu et al., 2016) as the evaluation dataset for this task. The dataset comprises 221k, 27k, and 27k images for training, validation, and testing. This benchmark encompasses five criteria: “texture”, “fabric”, “shape”, “part”, and “style”, containing 156, 218, 180, 216, and 230 distinct values, respectively.

Setup. For each query sample, we compute the cosine similarity between the query and all candidate samples. The candidate samples are then ranked in descending order of similarity, and retrieval performance is evaluated accordingly. To facilitate similarity-based retrieval, we leverage OD-CRL to generate criterion-specific representations for all samples, and these representations are further optimized by a two-layer MLP combined with triplet loss.

Metric. We adopt Mean Average Precision (mAP) as the evaluation metric for the customized fashion retrieval task.

Performance. Table 3 presents the performance comparison on customized fashion retrieval. Equipped with merely a simple MLP, our proposed CLIP+OD-CRL achieves the best

Table 2. Performance on the task of customized few-shot classification.

Method	Clevr4-10k						Cards						Mean	
	Shape			Color			number			suits				
	1	5	10	1	5	10	1	5	10	1	5	10		
CLIP	58.16	83.17	89.47	26.85	57.33	70.00	20.63	33.73	41.84	37.65	56.36	65.98	53.43	
CLIP+CRL	58.69	86.63	92.28	65.71	89.13	93.21	17.65	44.51	51.08	37.11	67.18	72.64	64.65	
CLIP+OD-CRL	68.81	90.26	94.83	82.43	91.43	93.42	33.50	49.55	54.28	52.58	71.79	76.45	71.61	
BLIP2	72.91	95.18	97.88	28.96	60.53	73.25	27.21	45.54	55.94	44.61	70.14	78.16	62.53	
BLIP2+CRL	71.53	94.94	98.00	59.73	85.34	91.04	26.44	61.64	70.14	50.44	79.91	84.13	72.77	
BLIP2+OD-CRL	88.21	97.75	98.69	78.44	88.74	91.47	48.60	68.39	73.81	71.24	82.44	84.41	81.02	

mean mAP of 10.26%. This result outperforms previous state-of-the-art methods, including Triplet (Veit et al., 2017), CSN (Veit et al., 2017), ASEN (Ma et al., 2020), ASEN++ (Dong et al., 2021), and RPF (Dong et al., 2023). Without training, CLIP+OD-CRL already surpasses vanilla CLIP by 34.54% in mean mAP, validating its effectiveness in generating discriminative criterion-specific representations.

Table 3. Performance on the task of customized fashion retrieval. The symbol \dagger signifies that training is conducted.

Method	Texture	Fabric	Shape	Part	Style	Mean
Triplet	13.26	6.28	9.49	4.43	3.33	7.36
CSN	14.09	6.39	11.07	5.13	3.49	8.01
ASEN	15.13	7.11	12.39	5.51	3.56	8.74
ASEN++	15.60	7.67	14.31	6.60	4.07	9.64
RPF	15.62	8.30	15.02	7.38	4.77	10.22
CLIP	9.14	4.68	7.86	4.26	4.48	6.08
CLIP+CRL	11.03	6.76	11.80	5.56	4.42	7.93
CLIP+CRL \dagger	13.53	7.70	<u>15.59</u>	6.69	<u>5.60</u>	9.94
CLIP+OD-CRL	11.04	6.74	12.46	5.69	4.95	8.18
CLIP+OD-CRL \dagger	13.88	7.88	16.05	<u>6.84</u>	6.14	10.26

4.4. Ablation Study

To validate the effectiveness of components in OD-CRL, we conduct ablation studies on the customized clustering task. Although customized clustering is one of downstream tasks for conditional representation learning, it provides the most direct assessment of representation quality. We perform the ablation experiments on the Clevr4-10k and Cards datasets.

As shown in Table 4, we systematically evaluate two key components: Adaptive Orthogonal Basis Optimization and Null-Space Denoising Projection. On Clevr4-10k, incorporating AOBO alone improves the shape clustering NMI from 78.40% to 82.37%, demonstrating that Adaptive Orthogonal Basis Optimization offers a higher-quality basis for disentangling different attributes. Incorporating NSDP further improves the NMI to 86.67%, as the null-space denoising projection effectively removes interference from

Table 4. Ablation study

Components		Clevr4-10k					
		Shape			Color		
AOBO	NSDP	NMI	ACC	ARI	NMI	ACC	ARI
		78.40	81.83	71.35	88.09	87.26	81.07
\checkmark		82.37	85.10	<u>77.32</u>	<u>88.13</u>	86.32	<u>81.24</u>
\checkmark	86.67	90.69	84.01	89.99	89.88	85.09	

Components		Cards					
		Number			Suits		
AOBO	NSDP	NMI	ACC	ARI	NMI	ACC	ARI
		24.68	28.59	12.27	37.70	62.08	34.36
\checkmark		38.03	<u>40.29</u>	<u>23.89</u>	39.69	70.45	<u>39.08</u>
\checkmark	38.78	44.45	28.40	41.61	73.22	42.20	

irrelevant semantic components within the noise subspace. Similar trends are observed on the Cards dataset, where the complete method consistently achieves the best performance across all metrics. These results confirm that both components are essential and complementary to OD-CRL’s overall performance.

4.5. Visualization

Figure 3 presents t-SNE visualizations of learned representations on the Clevr4-10k dataset under the “shape” (a-c) and “color” (d-f) criteria. CLIP’s general representations (a, d) exhibit severe entanglement across semantic categories, failing to capture criterion-specific distinctions. While CRL (b, e) shows improved cluster formation, considerable inter-cluster overlap persists. In contrast, OD-CRL (c, f) achieves well-separated and compact clusters across both criteria, demonstrating superior discriminative performance.

4.6. Analysis on Text Basis

In practical scenarios, the optimal number of text basis vectors remains unknown. To validate the robustness of

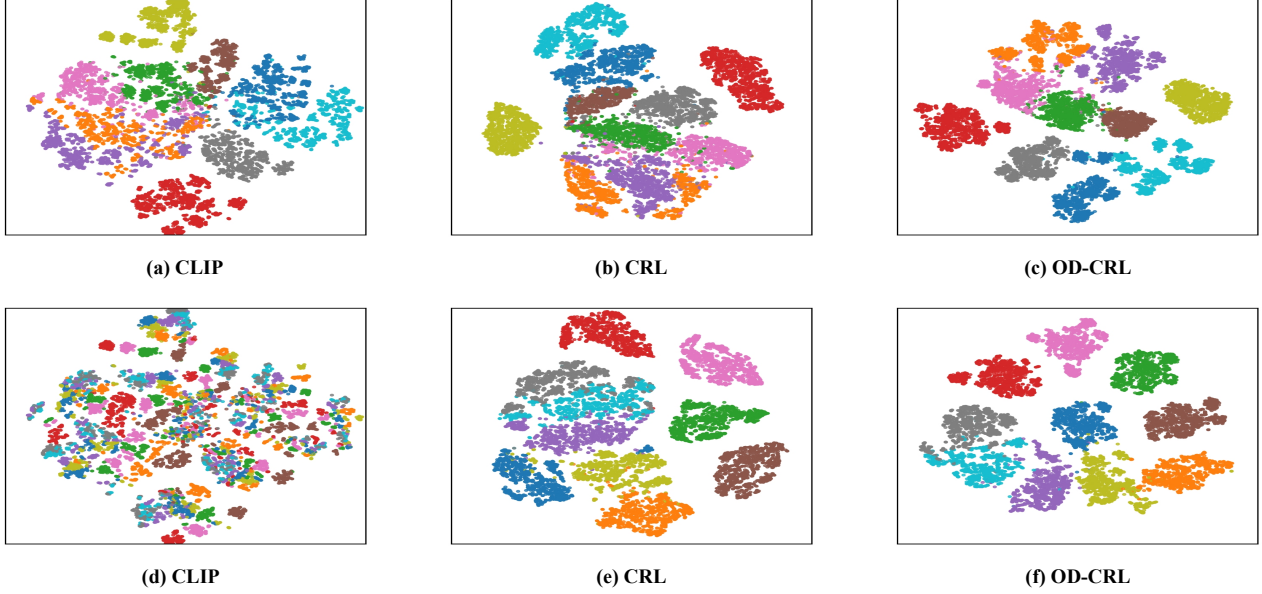


Figure 3. T-SNE visualizations of the representations learned by CLIP, CRL, and OD-CRL on the Clevr4-10k dataset for the “shape” criterion (a, b, c) and the “color” criterion (d, e, f).

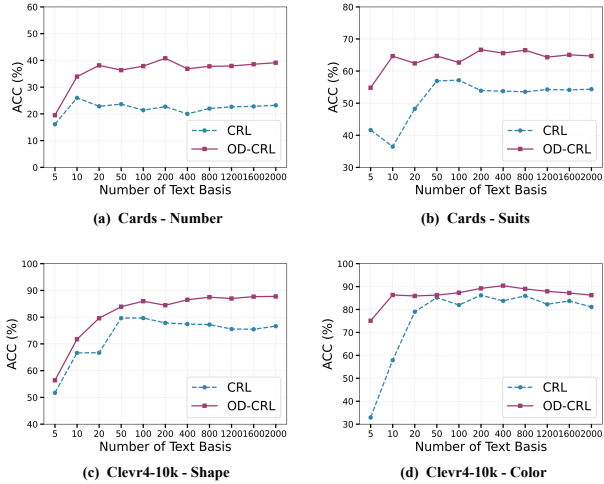


Figure 4. Performance with different numbers of basis vectors.

OD-CRL to text basis quantity, we examine its performance on the customized clustering task under varying numbers of basis vectors. As shown in Figure 4, we conduct experiments on both Clevr4-10k and Cards datasets with the number of basis vectors ranging from 5 to 2000.

OD-CRL exhibits stable and superior performance across all criteria, remaining insensitive to the number of basis vectors. In contrast, CRL demonstrates significant performance

variations, particularly in color-based clustering on Clevr4-10k. Moreover, regardless of the initial basis cardinality, OD-CRL utilizes only a small set of optimized basis vectors constructed through Adaptive Orthogonal Basis Optimization. This enables OD-CRL to achieve significant efficiency and performance advantages in scenarios where the semantics corresponding to the criterion are overly broad.

5. Conclusion

In this paper, We identify the key factors that influence the performance of existing conditional representation learning methods: (1) quality of LLM-generated text bases; (2) mutual interference between different conditional subspaces. To address these limitations, we propose OD-CRL, which combines Adaptive Orthogonal Basis Optimization and Null-Space Denoising Projection to extract conditional representations without task-specific training.

Extensive experiments on customized clustering, few-shot classification, and fashion retrieval demonstrate that OD-CRL outperforms existing methods across diverse evaluation criteria. Ablation studies confirm the effectiveness of each component, while robustness analysis reveals stable performance across varying numbers of basis vectors.

Given the growing importance of conditional representation learning, we hope that OD-CRL represents a significant step toward more efficient and flexible approaches in this domain.

Impact Statement

This paper presents work whose goal is to advance the field of Machine Learning. There are many potential societal consequences of our work, none which we feel must be specifically highlighted here.

References

Caron, M., Misra, I., Mairal, J., Goyal, P., Bojanowski, P., and Joulin, A. Unsupervised learning of visual features by contrasting cluster assignments. *Advances in neural information processing systems*, 33:9912–9924, 2020.

Chen, T., Kornblith, S., Norouzi, M., and Hinton, G. A simple framework for contrastive learning of visual representations. In *International conference on machine learning*, pp. 1597–1607. PMLR, 2020.

Devlin, J., Chang, M.-W., Lee, K., and Toutanova, K. Bert: Pre-training of deep bidirectional transformers for language understanding. In *Proceedings of the 2019 conference of the North American chapter of the association for computational linguistics: human language technologies, volume 1 (long and short papers)*, pp. 4171–4186, 2019.

Doersch, C., Gupta, A., and Efros, A. A. Unsupervised visual representation learning by context prediction. In *Proceedings of the IEEE international conference on computer vision*, pp. 1422–1430, 2015.

Dong, J., Ma, Z., Mao, X., Yang, X., He, Y., Hong, R., and Ji, S. Fine-grained fashion similarity prediction by attribute-specific embedding learning. *IEEE Transactions on Image Processing*, 30:8410–8425, 2021.

Dong, J., Peng, X., Ma, Z., Liu, D., Qu, X., Yang, X., Zhu, J., and Liu, B. From region to patch: Attribute-aware foreground-background contrastive learning for fine-grained fashion retrieval. In *Proceedings of the 46th International ACM SIGIR Conference on Research and Development in Information Retrieval*, pp. 1273–1282, 2023.

Geng, X., Zhao, S., Yu, Y., Peng, B., Du, P., Chen, H., Li, C., and Wang, M. Personalized clustering via targeted representation learning. In *Proceedings of the AAAI Conference on Artificial Intelligence*, volume 39, pp. 16790–16798, 2025.

Gidaris, S., Singh, P., and Komodakis, N. Unsupervised representation learning by predicting image rotations. *arXiv preprint arXiv:1803.07728*, 2018.

Gordo, A., Almazán, J., Revaud, J., and Larlus, D. Deep image retrieval: Learning global representations for image search. In *European conference on computer vision*, pp. 241–257. Springer, 2016.

He, K., Fan, H., Wu, Y., Xie, S., and Girshick, R. Momentum contrast for unsupervised visual representation learning. In *Proceedings of the IEEE/CVF conference on computer vision and pattern recognition*, pp. 9729–9738, 2020.

He, K., Chen, X., Xie, S., Li, Y., Dollár, P., and Girshick, R. Masked autoencoders are scalable vision learners. In *Proceedings of the IEEE/CVF conference on computer vision and pattern recognition*, pp. 16000–16009, 2022.

Hinton, G. E. and Salakhutdinov, R. R. Reducing the dimensionality of data with neural networks. *science*, 313 (5786):504–507, 2006.

Kingma, D. P. and Welling, M. Auto-encoding variational bayes. *arXiv preprint arXiv:1312.6114*, 2013.

Kwon, S., Park, J., Kim, M., Cho, J., Ryu, E. K., and Lee, K. Image clustering conditioned on text criteria. *arXiv preprint arXiv:2310.18297*, 2023.

Li, J., Li, D., Savarese, S., and Hoi, S. Blip-2: Bootstrapping language-image pre-training with frozen image encoders and large language models. In *International conference on machine learning*, pp. 19730–19742. PMLR, 2023.

Li, Y., Hu, P., Liu, Z., Peng, D., Zhou, J. T., and Peng, X. Contrastive clustering. In *Proceedings of the AAAI conference on artificial intelligence*, volume 35, pp. 8547–8555, 2021.

Liu, H., Hu, P., Zhang, C., Li, Y., and Peng, X. Interactive deep clustering via value mining. *Advances in Neural Information Processing Systems*, 37:42369–42387, 2024.

Liu, H., Sun, C., Hu, P., Li, Y., and Peng, X. Conditional representation learning for customized tasks. *arXiv preprint arXiv:2510.04564*, 2025.

Liu, Z., Luo, P., Qiu, S., Wang, X., and Tang, X. Deepfashion: Powering robust clothes recognition and retrieval with rich annotations. In *Proceedings of the IEEE conference on computer vision and pattern recognition*, pp. 1096–1104, 2016.

Ma, Z., Dong, J., Long, Z., Zhang, Y., He, Y., Xue, H., and Ji, S. Fine-grained fashion similarity learning by attribute-specific embedding network. In *Proceedings of the AAAI Conference on artificial intelligence*, volume 34, pp. 11741–11748, 2020.

Mo, Y., Peng, L., Xu, J., Shi, X., and Zhu, X. Simple unsupervised graph representation learning. In *Proceedings of the AAAI conference on artificial intelligence*, volume 36, pp. 7797–7805, 2022.

Noroози, M. and Favaro, P. Unsupervised learning of visual representations by solving jigsaw puzzles. In *European conference on computer vision*, pp. 69–84. Springer, 2016.

Radford, A., Kim, J. W., Hallacy, C., Ramesh, A., Goh, G., Agarwal, S., Sastry, G., Askell, A., Mishkin, P., Clark, J., et al. Learning transferable visual models from natural language supervision. In *International conference on machine learning*, pp. 8748–8763. PMLR, 2021.

Sarafianos, N., Xu, X., and Kakadiaris, I. A. Adversarial representation learning for text-to-image matching. In *Proceedings of the IEEE/CVF international conference on computer vision*, pp. 5814–5824, 2019.

Van Gansbeke, W., Vandenhende, S., Georgoulis, S., Proesmans, M., and Van Gool, L. Scan: Learning to classify images without labels. In *European conference on computer vision*, pp. 268–285. Springer, 2020.

Vaze, S., Vedaldi, A., and Zisserman, A. No representation rules them all in category discovery. *Advances in Neural Information Processing Systems*, 36:19962–19989, 2023.

Veit, A., Belongie, S., and Karaletsos, T. Conditional similarity networks. In *Proceedings of the IEEE conference on computer vision and pattern recognition*, pp. 830–838, 2017.

Vincent, P., Larochelle, H., Bengio, Y., and Manzagol, P.-A. Extracting and composing robust features with denoising autoencoders. In *Proceedings of the 25th international conference on Machine learning*, pp. 1096–1103, 2008.

Wang, X., Jia, Y., Liu, H., and Hou, J. Esmc: Mllm-based embedding selection for explainable multiple clustering. *arXiv preprint arXiv:2512.00725*, 2025.

Wei, C., Fan, H., Xie, S., Wu, C.-Y., Yuille, A., and Feichtenhofer, C. Masked feature prediction for self-supervised visual pre-training. In *Proceedings of the IEEE/CVF conference on computer vision and pattern recognition*, pp. 14668–14678, 2022.

Yan, S., Yang, Z., Li, H., Song, C., Guan, L., Kang, H., Hua, G., and Huang, Q. Implicit autoencoder for point-cloud self-supervised representation learning. In *Proceedings of the IEEE/CVF International Conference on Computer Vision*, pp. 14530–14542, 2023.

Yao, J., Liu, E., Rashid, M., and Hu, J. Augdmc: Data augmentation guided deep multiple clustering. *Procedia Computer Science*, 222:571–580, 2023.

Yao, J., Qian, Q., and Hu, J. Customized multiple clustering via multi-modal subspace proxy learning. *Advances in Neural Information Processing Systems*, 37:82705–82725, 2024a.

Yao, J., Qian, Q., and Hu, J. Multi-modal proxy learning towards personalized visual multiple clustering. In *Proceedings of the IEEE/CVF Conference on Computer Vision and Pattern Recognition*, pp. 14066–14075, 2024b.

Zhang, R., Isola, P., and Efros, A. A. Colorful image colorization. In *European conference on computer vision*, pp. 649–666. Springer, 2016.

A. Datasets and Corresponding Prompts

In this section, we provide detailed descriptions of the datasets used in our experiments, along with the corresponding prompts for LLM and VLM. We organize the content by dataset, presenting the dataset structure and the specific prompts employed for each criterion.

A.1. Clevr4-10k

A.1.1. DATASET STRUCTURE

Clevr4-10k (Vaze et al., 2023) is a synthetic benchmark dataset built upon the CLEVR dataset. It consists of 10,531 images featuring multiple 3D objects positioned within fixed scenes. Each image in Clevr4-10k is annotated with all four criteria simultaneously, allowing for comprehensive evaluation of conditional representation learning methods. Table 5 shows the structure of the Clevr4-10k dataset.

Table 5. Structure of the Clevr4-10k dataset.

Criterion	Number of Classes	Class Examples
Shape	10	cone, cube, cylinder, diamond, gear, ...
Texture	10	brick, checkered, chessboard, circles, emojis, ...
Color	10	blue, brown, cyan, gray, green, ...
Count	10	1, 2, 3, 4, 5, ...

A.1.2. LLM PROMPTS

For Clevr4-10k, we design criterion-specific prompts to query the LLM for generating descriptive texts. Below we present the prompts used for each criterion:

Please generate common expressions to describe the shape (Texture / Color / Count), as many as possible, formatted as: `["...", "...", "..."]`. Ensure all items are unique and written in a single line, without any nested lists or additional formatting. Only generate the list, and do not include any additional information.

A.1.3. VLM PROMPTS

For encoding the LLM-generated texts using the VLM, we construct prompts that combine the criterion with each descriptive text. The general template is:

Objects with the [CRITERION] of [TEXT].

where [CRITERION] is replaced with the specific criterion (e.g., “shape”, “texture”, “color”, “count”) and [TEXT] is replaced with each generated descriptive text.

A.2. Cards

A.2.1. DATASET STRUCTURE

The Cards dataset (Yao et al., 2023) is a poker card image dataset comprising 8,029 images of playing cards. Each card is photographed under various conditions, providing natural variations in lighting, angle, and background. Table 6 shows the structure of the Cards dataset.

Table 6. Structure of the Cards dataset.

Criterion	Number of Classes	Class Examples
Number	13	Ace, Two, three, ..., Jack, Queen, King
Suit	4	Clubs(♣), Diamonds(♦), Hearts(♥), Spades(♠)

A.2.2. LLM PROMPTS

For Cards, we design criterion-specific prompts to query the LLM for generating descriptive texts. Below we present the prompts used for each criterion:

Please generate common expressions to describe the number (suit) of playing cards, as many as possible, formatted as: `["...", "...", "..."]`. Ensure all items are unique and written in a single line, without any nested lists or additional formatting. Only generate the list, and do not include any additional information.

A.2.3. VLM PROMPTS

For encoding the LLM-generated texts using the VLM, we construct prompts that combine the criterion with each descriptive text. The general template is:

A poker card with the [CRITERION] of [TEXT].

where [CRITERION] is replaced with the specific criterion (e.g., “number”, “suit”) and [TEXT] is replaced with each generated descriptive text.

A.3. DeepFashion

A.3.1. DATASET STRUCTURE

DeepFashion (Liu et al., 2016) is a large-scale fashion dataset widely used for clothing-related computer vision tasks. Following previous works (Ma et al., 2020), we use the category and attribute prediction benchmark split, which consists of 221,000 training images, 27,000 validation images, and 27,000 test images. Each image in DeepFashion is annotated with multiple attribute criteria simultaneously. Table 7 shows the structure of the DeepFashion dataset.

Table 7. Structure of the DeepFashion dataset.

Criterion	Number of Classes	Class Examples
Texture	156	abstract, animal, baroque, camo, circle, ...
Fabric	218	acid, bead, canvas, cloud, feather, ...
Shape	180	a-line, boxy, cropped, flared, shirt, ...
Part	216	bell, bow, buttoned, cowl, flat, ...
Style	230	baseball, bike, eagle, fox, mickey, ...

A.3.2. LLM PROMPTS

For DeepFashion, we design criterion-specific prompts to query the LLM for generating descriptive texts. Below we present the prompts used for each criterion:

Please generate common expressions to describe the texture (fabric / shape / part / style) of fashion items, as many as possible, formatted as: `["...", "...", "..."]`. Ensure all items are unique and written in a single line, without any nested lists or additional formatting. Only generate the list, and do not include any additional information.

A.3.3. VLM PROMPTS

For encoding the LLM-generated texts using the VLM, we construct prompts that combine the criterion with each descriptive text. The general template is:

A fashion with the [CRITERION] of [TEXT].

where [CRITERION] is replaced with the specific criterion (e.g., “texture”, “fabric”, “shape”, “part”, “style”) and [TEXT] is replaced with each generated descriptive text.

B. Theoretical Analysis of Null-Space Denoising Projection

In this section, we provide a theoretical analysis demonstrating that the benefits of Null-Space Denoising Projection (noise reduction) substantially outweigh its costs (partial loss of target semantics).

B.1. Preliminaries and Notation

Recall that the image embedding admits the decomposition:

$$\mathbf{I} = \mathbf{R}_t \mathbf{T}_t^* + \mathbf{R}_n \mathbf{T}_n^* + \boldsymbol{\epsilon} \quad (16)$$

where $\mathbf{T}_t^* \in \mathbb{R}^{k^* \times d}$ and $\mathbf{T}_n^* \in \mathbb{R}^{p \times d}$ are orthonormal bases satisfying:

$$\mathbf{T}_t^*(\mathbf{T}_t^*)^\top = \mathbf{I}_{k^*}, \quad \mathbf{T}_n^*(\mathbf{T}_n^*)^\top = \mathbf{I}_p \quad (17)$$

We define the projection matrices onto the target and noise subspaces as:

$$\mathbf{P}_t = (\mathbf{T}_t^*)^\top \mathbf{T}_t^*, \quad \mathbf{P}_n = (\mathbf{T}_n^*)^\top \mathbf{T}_n^* \quad (18)$$

Through Adaptive Orthogonal Basis Optimization, the target and noise subspaces are approximately orthogonal but not perfectly so. We quantify their non-orthogonality by:

$$\left\| \mathbf{T}_t^*(\mathbf{T}_n^*)^\top \right\| = \left\| \mathbf{T}_n^*(\mathbf{T}_t^*)^\top \right\| = \epsilon \ll 1 \quad (19)$$

where $\|\cdot\|$ denotes the spectral norm.

For notational convenience, we define the cross-subspace coupling matrix:

$$\mathbf{A} = \mathbf{T}_t^*(\mathbf{T}_n^*)^\top \in \mathbb{R}^{k^* \times p}, \quad \text{with } \|\mathbf{A}\| = \epsilon \quad (20)$$

B.2. Quantifying Benefits and Costs

We analyze the effects of null-space projection by examining two quantities:

Benefit (Noise Reduction): The interference from the noise component $\mathbf{R}_n \mathbf{T}_n^*$ that would otherwise leak into the target subspace is characterized by:

$$\mathcal{B} = \left\| \mathbf{R}_n \mathbf{T}_n^*(\mathbf{T}_t^*)^\top \right\|_F \quad (21)$$

Cost (Signal Loss): The target-aligned component $\mathbf{R}_t \mathbf{T}_t^*$ that is inadvertently removed due to its partial overlap with the noise subspace is characterized by:

$$\mathcal{C} = \left\| \mathbf{R}_t \mathbf{T}_t^* \mathbf{P}_n(\mathbf{T}_t^*)^\top \right\|_F \quad (22)$$

B.3. Detailed Derivations

Lemma B.1 (Benefit Term Expansion). *The noise leakage term can be expressed as:*

$$\mathbf{R}_n \mathbf{T}_n^*(\mathbf{T}_t^*)^\top = \mathbf{R}_n \mathbf{A}^\top \quad (23)$$

Proof. By direct substitution using $\mathbf{A}^\top = \mathbf{T}_n^*(\mathbf{T}_t^*)^\top$:

$$\mathbf{R}_n \mathbf{T}_n^*(\mathbf{T}_t^*)^\top = \mathbf{R}_n \mathbf{A}^\top \quad (24)$$

■

Lemma B.2 (Cost Term Expansion). *The signal loss term can be expressed as:*

$$\mathbf{R}_t \mathbf{T}_t^* \mathbf{P}_n(\mathbf{T}_t^*)^\top = \mathbf{R}_t \mathbf{A} \mathbf{A}^\top \quad (25)$$

Proof. Expanding $\mathbf{P}_n = (\mathbf{T}_n^*)^\top \mathbf{T}_n^*$:

$$\mathbf{R}_t \mathbf{T}_t^* \mathbf{P}_n(\mathbf{T}_t^*)^\top = \mathbf{R}_t \mathbf{T}_t^* (\mathbf{T}_n^*)^\top \mathbf{T}_n^*(\mathbf{T}_t^*)^\top \quad (26)$$

$$= \mathbf{R}_t \underbrace{\mathbf{T}_t^* (\mathbf{T}_n^*)^\top}_{\mathbf{A}} \underbrace{\mathbf{T}_n^*(\mathbf{T}_t^*)^\top}_{\mathbf{A}^\top} \quad (27)$$

$$= \mathbf{R}_t \mathbf{A} \mathbf{A}^\top \quad (28)$$

■

B.4. Main Theorem

Theorem B.3 (Benefit-Cost Ratio of Null-Space Denoising). *Under the approximately orthogonal subspace assumption with $\|\mathbf{A}\| = \|\mathbf{T}_t^*(\mathbf{T}_n^*)^\top\| = \epsilon \ll 1$, the ratio of noise reduction benefit to signal loss cost satisfies:*

$$\frac{\mathcal{B}}{\mathcal{C}} \geq \frac{\|\mathbf{R}_n\|_F}{\|\mathbf{R}_t\|_F} \cdot \frac{1}{\epsilon} \quad (29)$$

When the target and noise components have comparable magnitudes ($\|\mathbf{R}_t\|_F \approx \|\mathbf{R}_n\|_F$), this ratio scales as $\mathcal{O}(1/\epsilon) \gg 1$.

Proof. We derive bounds for both \mathcal{B} and \mathcal{C} using the expressions from Lemmas B.1 and B.2.

Benefit Analysis. From Lemma B.1:

$$\mathcal{B} = \|\mathbf{R}_n \mathbf{A}^\top\|_F \quad (30)$$

To establish a lower bound, we use the property that for any matrices \mathbf{X} and \mathbf{Y} :

$$\|\mathbf{X}\mathbf{Y}\|_F \geq \sigma_{\min}(\mathbf{Y})\|\mathbf{X}\|_F \quad (31)$$

where $\sigma_{\min}(\mathbf{Y})$ denotes the smallest singular value.

For typical noise components that are not degenerate with respect to the cross-subspace coupling, we have:

$$\mathcal{B} = \|\mathbf{R}_n \mathbf{A}^\top\|_F \sim \|\mathbf{R}_n\|_F \cdot \|\mathbf{A}^\top\| = \|\mathbf{R}_n\|_F \cdot \epsilon \quad (32)$$

More precisely, under the assumption that \mathbf{R}_n has non-trivial components along the directions captured by \mathbf{A}^\top :

$$\mathcal{B} \gtrsim c_1 \|\mathbf{R}_n\|_F \cdot \epsilon \quad (33)$$

for some constant $0 < c_1 < 1$ of order unity.

Cost Analysis. From Lemma B.2:

$$\mathcal{C} = \|\mathbf{R}_t \mathbf{A} \mathbf{A}^\top\|_F \quad (34)$$

Using the submultiplicativity of the Frobenius norm with respect to the spectral norm:

$$\|\mathbf{X}\mathbf{Y}\|_F \leq \|\mathbf{X}\|_F \cdot \|\mathbf{Y}\| \quad (35)$$

we obtain:

$$\mathcal{C} = \|\mathbf{R}_t \mathbf{A} \mathbf{A}^\top\|_F \quad (36)$$

$$\leq \|\mathbf{R}_t\|_F \cdot \|\mathbf{A} \mathbf{A}^\top\| \quad (37)$$

$$\leq \|\mathbf{R}_t\|_F \cdot \|\mathbf{A}\| \cdot \|\mathbf{A}^\top\| \quad (38)$$

$$= \|\mathbf{R}_t\|_F \cdot \epsilon^2 \quad (39)$$

Note that $\|\mathbf{A} \mathbf{A}^\top\| = \|\mathbf{A}\|^2 = \epsilon^2$ since $\mathbf{A} \mathbf{A}^\top$ is positive semidefinite and its spectral norm equals its largest eigenvalue, which is $\sigma_{\max}^2(\mathbf{A}) = \epsilon^2$.

Ratio Bound. Combining the benefit lower bound and cost upper bound:

$$\frac{\mathcal{B}}{\mathcal{C}} \geq \frac{c_1 \|\mathbf{R}_n\|_F \cdot \epsilon}{\|\mathbf{R}_t\|_F \cdot \epsilon^2} = c_1 \cdot \frac{\|\mathbf{R}_n\|_F}{\|\mathbf{R}_t\|_F} \cdot \frac{1}{\epsilon} \quad (40)$$

Taking $c_1 \sim 1$ for typical configurations yields the stated bound. ■

B.5. Geometric Interpretation

The theoretical analysis reveals a fundamental asymmetry in cross-subspace interference:

- **Noise Contamination** ($\mathcal{O}(\epsilon)$): The noise component $\mathbf{R}_n \mathbf{T}_n^*$ leaks into the target subspace through a single cross-subspace mapping $\mathbf{A}^\top = \mathbf{T}_n^* (\mathbf{T}_t^*)^\top$, incurring first-order interference proportional to ϵ .
- **Signal Loss** ($\mathcal{O}(\epsilon^2)$): The target component $\mathbf{R}_t \mathbf{T}_t^*$ loses information only through the round-trip mapping $\mathbf{A} \mathbf{A}^\top = \mathbf{T}_t^* (\mathbf{T}_n^*)^\top \mathbf{T}_n^* (\mathbf{T}_t^*)^\top$, which first projects onto the noise subspace and then back. This double passage through the ϵ -coupling results in second-order loss proportional to ϵ^2 .

This order-of-magnitude difference ensures that Null-Space Denoising Projection achieves substantial noise suppression while preserving the majority of target-relevant semantics, particularly when the subspaces exhibit low mutual coherence ($\epsilon \ll 1$).